Supplemental Material: SRC-2 is an essential coactivator for orchestrating metabolism and circadian rhythm

Erin Stashi, Rainer B. Lanz, Jianqiang Mao, George Michailidis, Bokai Zhu, Nicole M. Kettner, Nagireddy Putluri, Erin L. Reineke, Lucas C. Reineke, Subhamoy Dasgupta, Adam Dean, Connor R. Stevenson, Natarajan Sivasubramanian, Arun Sreekumar, Francesco DeMayo , Brian York, Loning Fu and Bert W. O'Malley

Figure S1

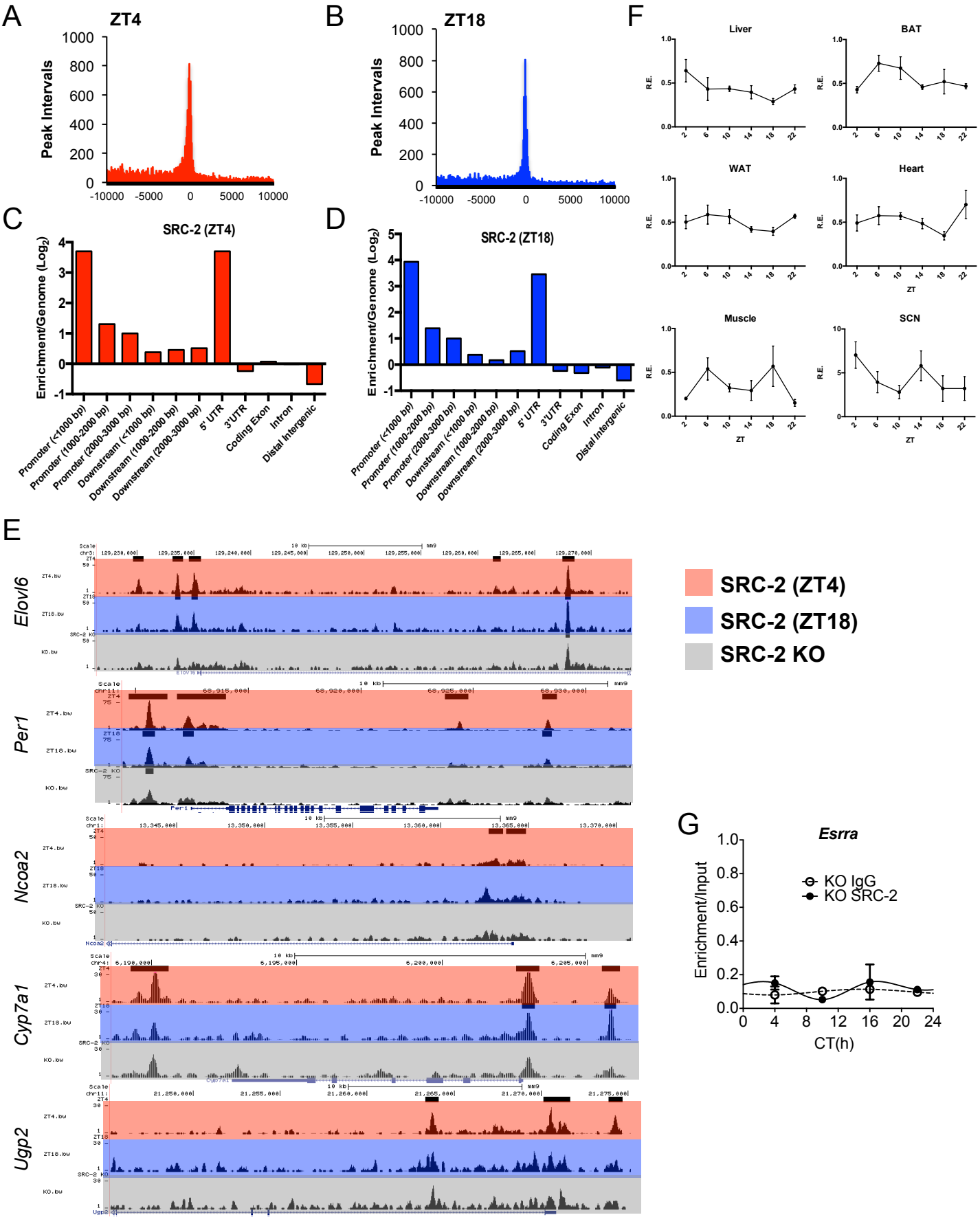
A
ZT4
Peak Intervals
B
ZT18
Peak Intervals
C
SRC-2 (ZT4)
Enrichment/Genome (Log2)
Promoter (<1000 bp)
Promoter (1000-2000 bp)
Promoter (2000-3000 bp)
Downstream (<1000 bp)
Downstream (1000-2000 bp)
Downstream (2000-3000 bp)
5' UTR
3'UTR
Coding Exon
Intron
Distal Intergenic
D
SRC-2 (ZT18)
Enrichment/Genome (Log2)
F
Liver
BAT
WAT
Heart
Muscle
SCN
R.E.
ZT
E
Elovl6
Per1
Ncoa2
Cyp7a1
Ugp2
SRC-2 (ZT4)
SRC-2 (ZT18)
SRC-2 KO
G
Esrra
KO IgG
KO SRC-2
Enrichment/Input
CT(h)

Figure S2

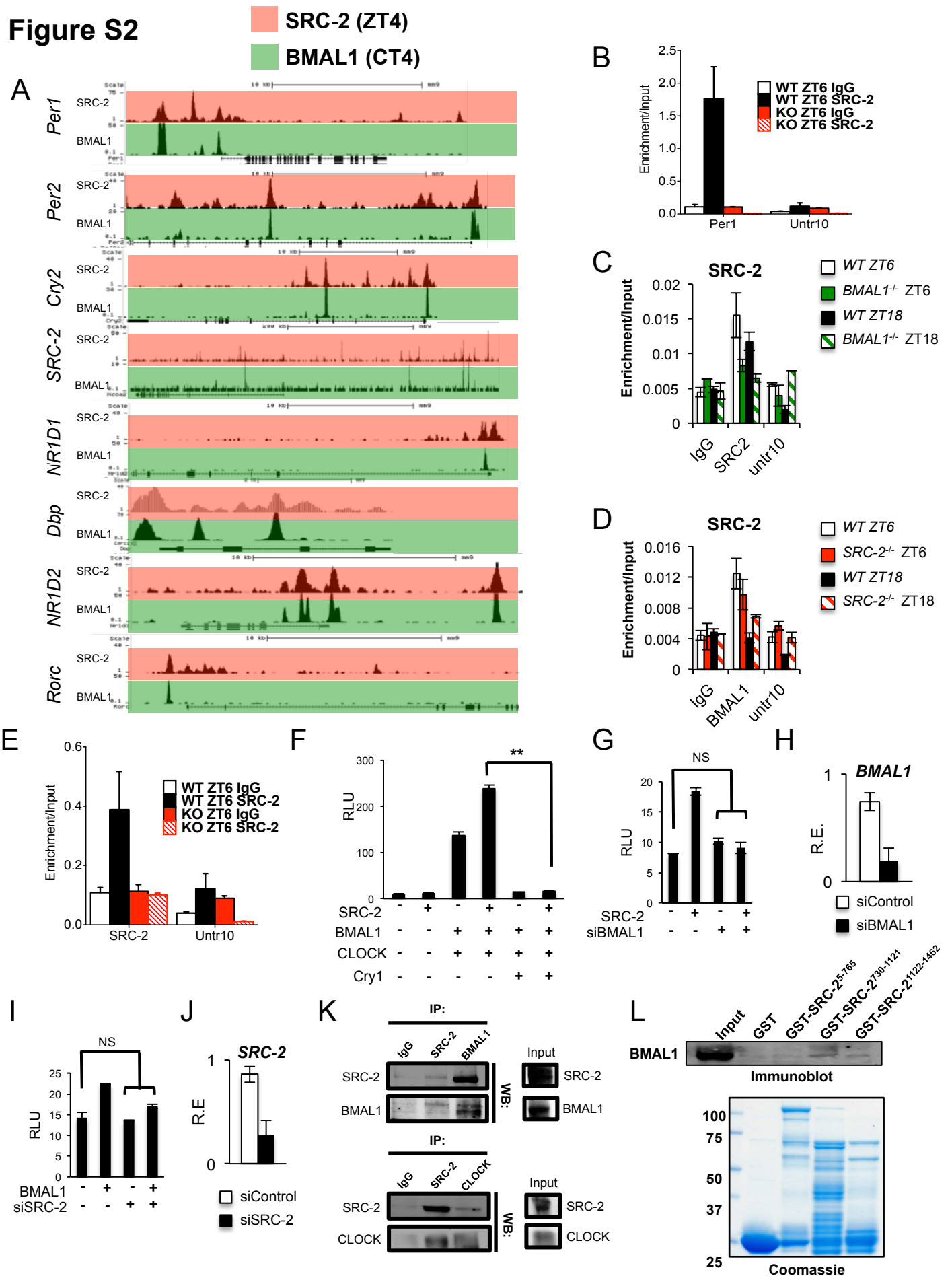
SRC-2 (ZT4)
BMAL1 (CT4)
A
Per1
Per2
Cry2
SRC-2
NR1D1
Dbp
NR1D2
Rorc
SRC-2
BMAL1
B
Enrichment/Input
WT ZT6 IgG
WT ZT6 SRC-2
KO ZT6 IgG
KO ZT6 SRC-2
Per1
Untr10
C
SRC-2
Enrichment/Input
WT ZT6
BMAL1-/- ZT6
WT ZT18
BMAL1-/- ZT18
IgG
SRC2
untr10
D
SRC-2
Enrichment/Input
WT ZT6
SRC-2-/- ZT6
WT ZT18
SRC-2-/- ZT18
IgG
BMAL1
untr10
E
Enrichment/Input
WT ZT6 IgG
WT ZT6 SRC-2
KO ZT6 IgG
KO ZT6 SRC-2
SRC-2
Untr10
F
RLU
**
SRC-2
BMAL1
CLOCK
Cry1
G
NS
RLU
SRC-2
siBMAL1
H
BMAL1
R.E.
siControl
siBMAL1
I
NS
RLU
BMAL1
siSRC-2
J
SRC-2
R.E
siControl
siSRC-2
K
IP:
IgG
SRC-2
BMAL1
SRC-2
BMAL1
WB:
Input
SRC-2
BMAL1
IP:
IgG
SRC-2
CLOCK
SRC-2
CLOCK
WB:
Input
SRC-2
CLOCK
L
Input
GST
GST-SRC-2 5-765
GST-SRC-2 730-1121
GST-SRC-2 1122-1462
BMAL1
Immunoblot
100
75
50
37
25
Coomassie

Figure S3

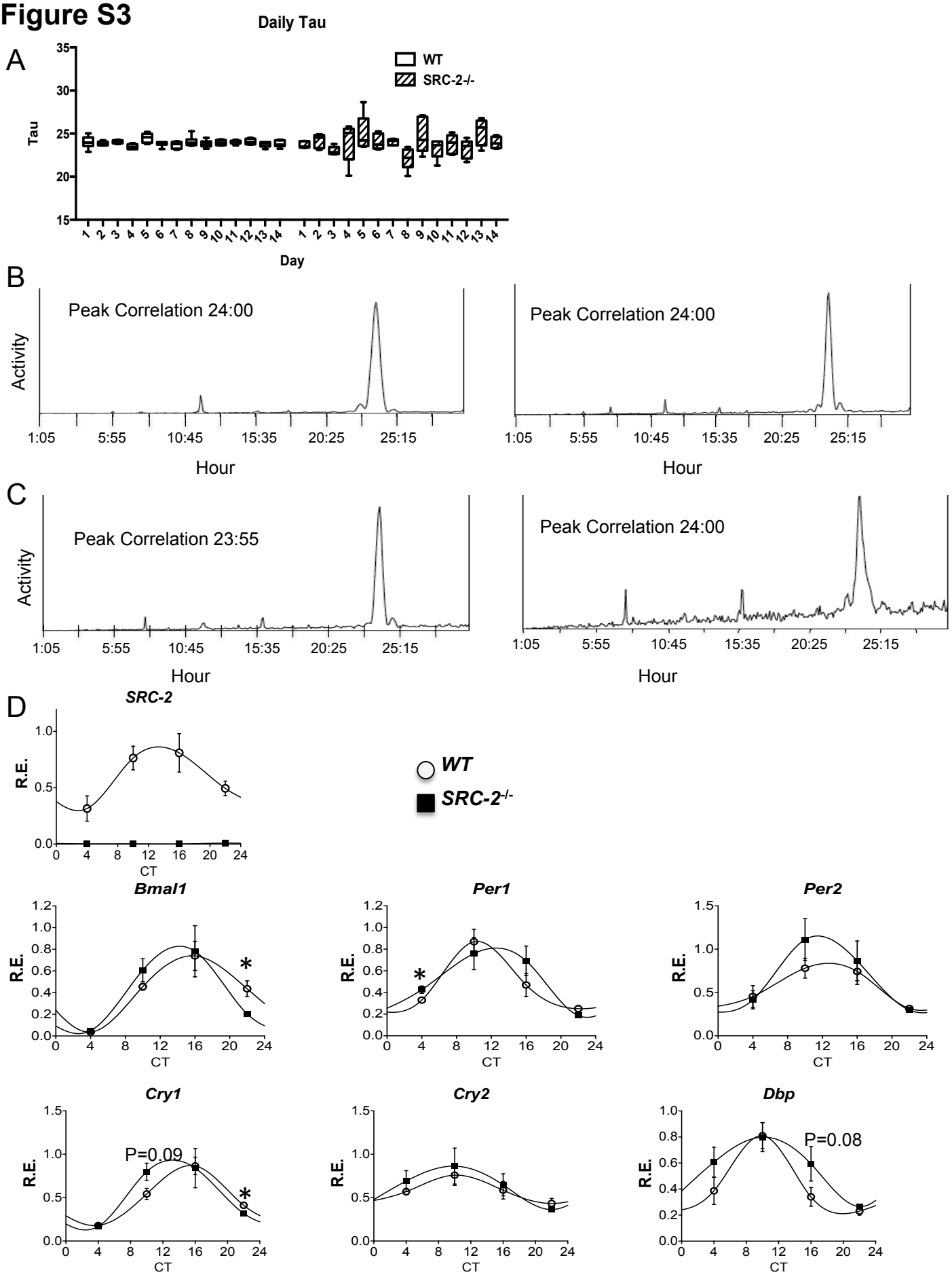
Daily Tau
A
WT
SRC-2-/-
Tau
Day
B
Peak Correlation 24:00
Activity
Hour
Peak Correlation 24:00
Hour
C
Peak Correlation 23:55
Activity
Hour
Peak Correlation 24:00
Hour
D
SRC-2
R.E.
CT
WT
SRC-2-/-
Bmal1
Per1
Per2
Cry1
P=0.09
Cry2
Dbp
P=0.08

Figure S4

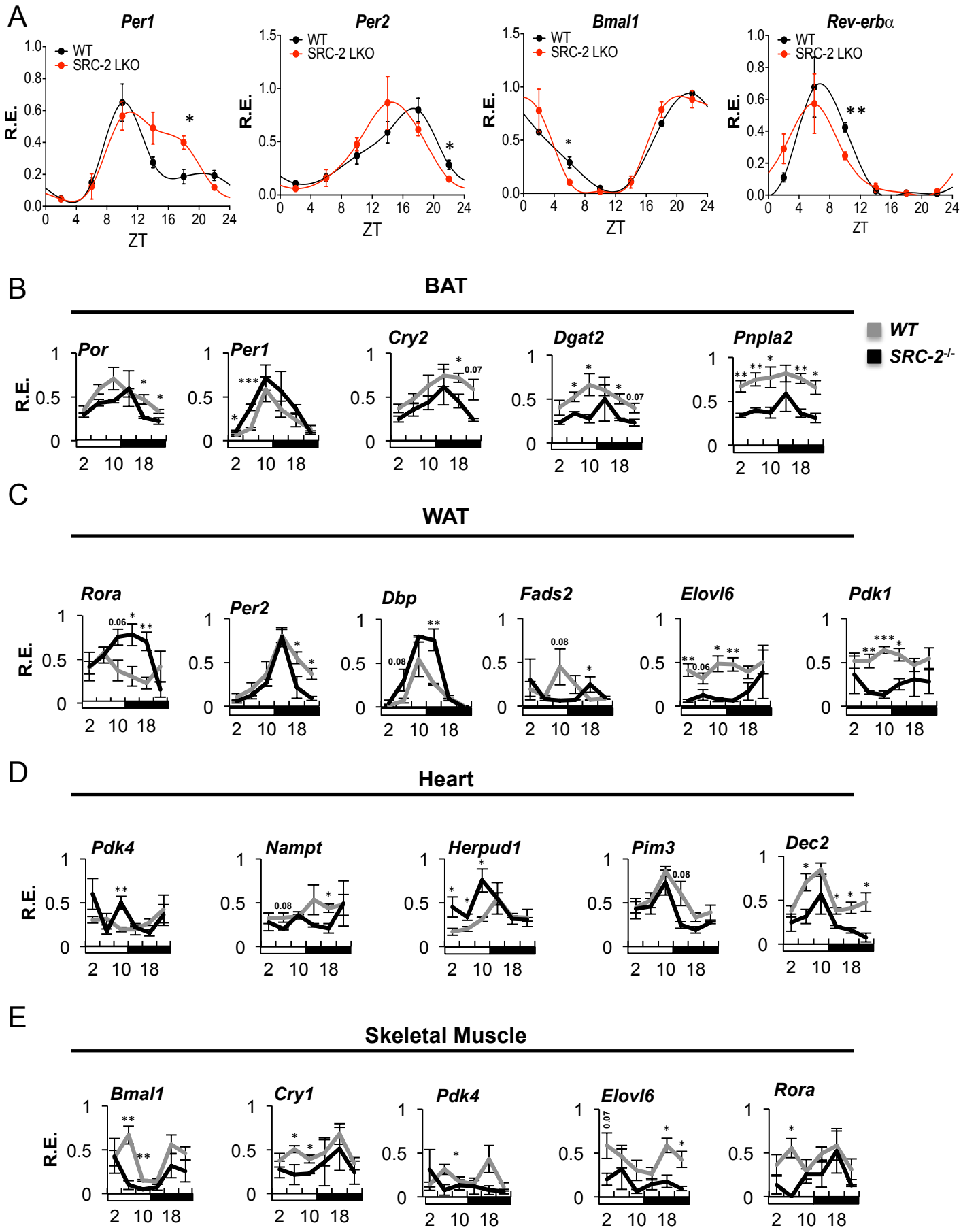
A
Per1
Per2
Bmal1
Rev-erbα
WT
SRC-2 LKO
R.E.
ZT
B
BAT
Por
Per1
Cry2
Dgat2
Pnpla2
WT
SRC-2-/-
C
WAT
Rora
Per2
Dbp
Fads2
Elovl6
Pdk1
D
Heart
Pdk4
Nampt
Herpud1
Pim3
Dec2
E
Skeletal Muscle
Bmal1
Cry1
Pdk4
Elovl6
Rora

Figure S5

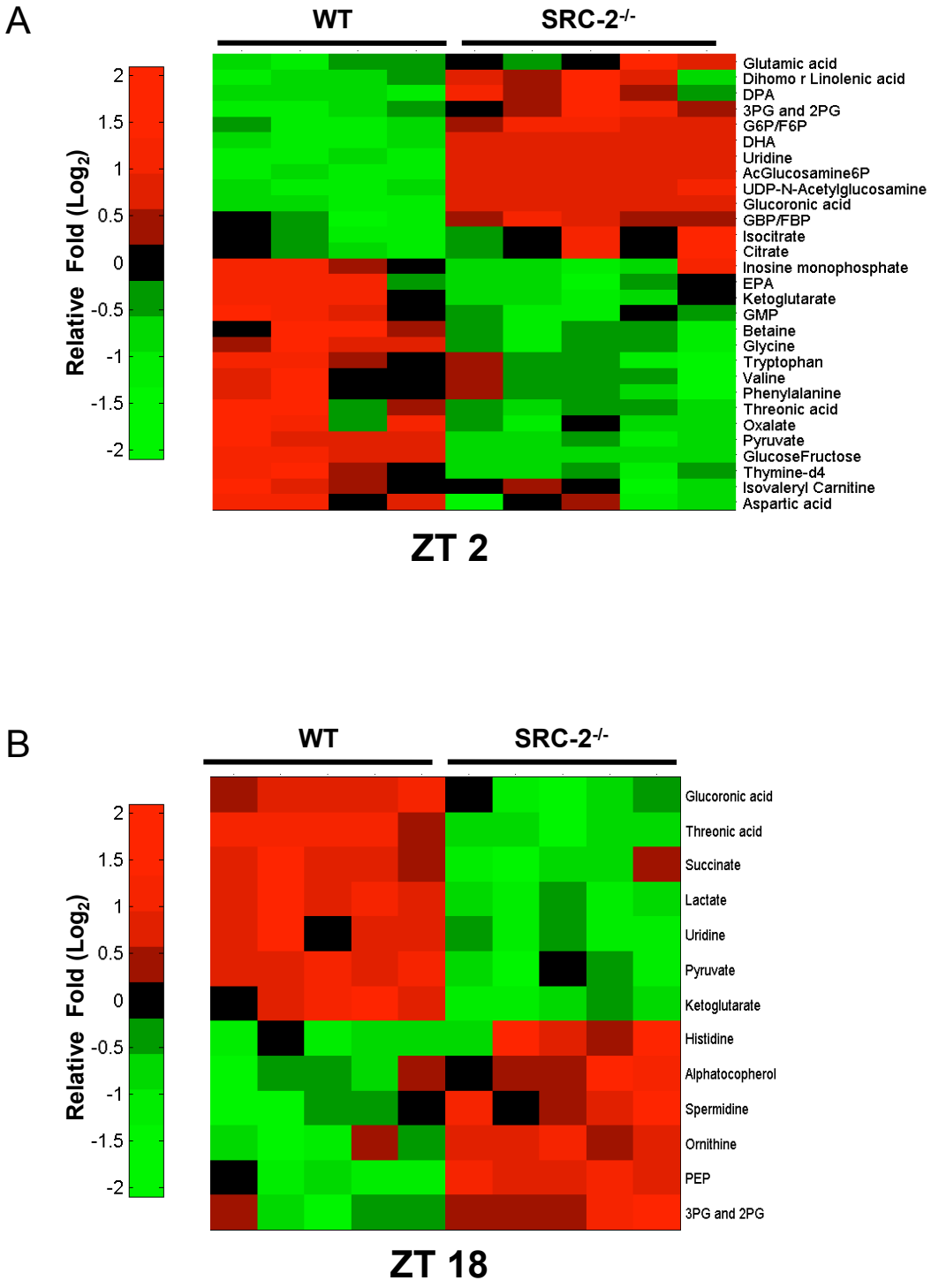
A
WT
SRC-2-/-
Relative Fold (Log2)
2
1.5
1
0.5
0
-0.5
-1
-1.5
-2
Glutamic acid
Dihomo r Linolenic acid
DPA
3PG and 2PG
G6P/F6P
DHA
Uridine
AcGlucosamine6P
UDP-N-Acetylglucosamine
Glucoronic acid
GBP/FBP
Isocitrate
Citrate
Inosine monophosphate
EPA
Ketoglutarate
GMP
Betaine
Glycine
Tryptophan
Valine
Phenylalanine
Threonic acid
Oxalate
Pyruvate
GlucoseFructose
Thymine-d4
Isovaleryl Carnitine
Aspartic acid
ZT 2
B
WT
SRC-2-/-
Relative Fold (Log2)
2
1.5
1
0.5
0
-0.5
-1
-1.5
-2
Glucoronic acid
Threonic acid
Succinate
Lactate
Uridine
Pyruvate
Ketoglutarate
Histidine
Alphatocopherol
Spermidine
Ornithine
PEP
3PG and 2PG
ZT 18

Figure S6

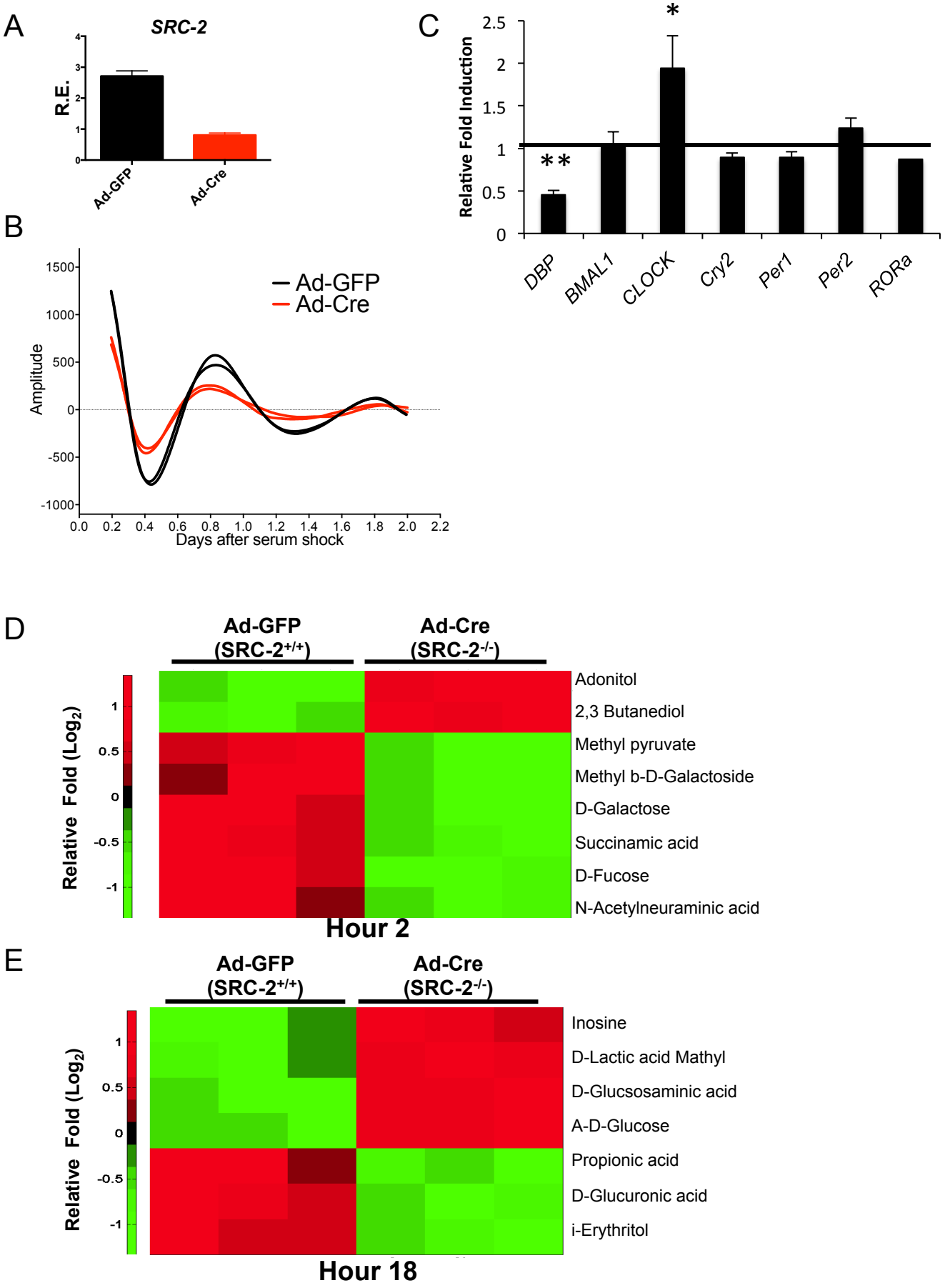
A
SRC-2
R.E.
Ad-GFP
Ad-Cre
B
Ad-GFP
Ad-Cre
Amplitude
Days after serum shock
C
Relative Fold Induction
DBP
BMAL1
CLOCK
Cry2
Per1
Per2
RORa
D
Ad-GFP (SRC-2+/+)
Ad-Cre (SRC-2-/-)
Relative Fold (Log2)
Adonitol
2,3 Butanediol
Methyl pyruvate
Methyl b-D-Galactoside
D-Galactose
Succinamic acid
D-Fucose
N-Acetylneuraminic acid
Hour 2
E
Ad-GFP (SRC-2+/+)
Ad-Cre (SRC-2-/-)
Relative Fold (Log2)
Inosine
D-Lactic acid Mathyl
D-Glucsosaminic acid
A-D-Glucose
Propionic acid
D-Glucuronic acid
i-Erythritol
Hour 18

Table S1

GeneID	Gene Symbol	Description	Synonyms
11865	Arntl	aryl hydrocarbon receptor nuclear translocator-like	Arnt3|BMAL1b|Bmal1|MOP3|bHLHe5|bmal1b'
20893	Bhlhe40	basic helix-loop-helix family, member e40	Bhlhb2|C130042M06Rik|CR8|Clast5|Dec1|Sharp2|Stra13|Stra14
79362	Bhlhe41	basic helix-loop-helix family, member e41	Bhlhb2l|Bhlhb3|DEC2|Sharp1
12753	Clock	circadian locomotor output cycles kaput	5330400M04Rik|KAT13D|bHLHe8|mKIAA0334
12952	Cry1	cryptochrome 1 (photolyase-like)	AU020726|AU021000|Phll1
12953	Cry2	cryptochrome 2 (photolyase-like)	AV006279|D130054K12Rik
104318	Csnk1d	casein kinase 1, delta	1200006A05Rik|AA409348|D930010H05Rik
13170	Dbp	D site albumin promoter binding protein	-
67800	Dgat2	diacylglycerol O-acyltransferase 2	0610010B06Rik|DGAT-2
170439	Elovl6	ELOVL family member 6, elongation of long chain fatty acids (yeast)	C77826|FAE|LCE|MGC107467
26379	Esrra	estrogen related receptor, alpha	ERRalpha|Err1|Estrra|Nr3b1
56473	Fads2	fatty acid desaturase 2	2900042M13Rik|Fadsd2
14118	Fbn1	fibrillin 1	AI536462|B430209H23|Fib-1|Tsk
14377	G6pc	glucose-6-phosphatase, catalytic	AW107337|G6Pase|G6pt|Glc-6-Pase
232493	Gys2	glycogen synthase 2	BC021322|LGS|MGC29379
64209	Herpud1	homocysteine-inducible, endoplasmic reticulum stress-inducible, ubiquitin-like domain member 1	Herp|Mifl|SUP
55927	Hes6	hairy and enhancer of split 6 (Drosophila)	AI326893|bHLHb41
15378	Hnf4a	hepatic nuclear factor 4, alpha	HNF-4|Hnf4|Hnf4alpha|MODY1|Nr2a1|Tcf14
16828	Ldha	lactate dehydrogenase A	Ldh1|Ldhm|l7R2
59027	Nampt	nicotinamide phosphoribosyltransferase	1110035O14Rik|AI314458|AI480535|NAmPRTase|Pbef|Pbef1|Visfatin
18030	Nfil3	nuclear factor, interleukin 3, regulated	AV225605|E4BP4
17977	Ncoa1	nuclear receptor coactivator 1	KAT13A|SRC-1|SRC1|bHLHe74
17978	Ncoa2	nuclear receptor coactivator 2	530095N19|D1Ertd433e|GRIP-1|Grip1|KAT13C|SRC-2|TIF-2|TIF2|bHLHe75
17979	Ncoa3	nuclear receptor coactivator 3	RP23-120P1.1|2010305B15Rik|AW321064|Actr|Aib1|KAT13B|Rac3|Src3|Tram-1|Tram1|bHLHe42|p/Cip|pCip
18143	Npas2	neuronal PAS domain protein 2	MGC129355|MOP4|bHLHe9
23957	Nr0b2	nuclear receptor subfamily 0, group B, member 2	SHP|SHP-1|Shp1
217166	Nr1d1	nuclear receptor subfamily 1, group D, member 1	A530070C09Rik|R75201
353187	Nr1d2	nuclear receptor subfamily 1, group D, member 2	RVR|Rev-erb
11819	Nr2f2	nuclear receptor subfamily 2, group F, member 2	2700033K02Rik|9430015G03Rik|ARP-1|Aporp1|COUP-TF2|COUP-TFII|COUPTFB|EAR3|SVP40|Tcfcoup2
26424	Nr5a2	nuclear receptor subfamily 5, group A, member 2	AU020803|D1Ertd308e|Ftf|LRH-1
18534	Pck1	phosphoenolpyruvate carboxykinase 1, cytosolic	AI265463|PEPCK|Pck-1
18563	Pcx	pyruvate carboxylase	Pc|Pcb
228026	Pdk1	pyruvate dehydrogenase kinase, isoenzyme 1	B830012B01|D530020C15Rik
27273	Pdk4	pyruvate dehydrogenase kinase, isoenzyme 4	AV005916
18626	Per1	period homolog 1 (Drosophila)	MGC102121|Per|m-rigui|mPer1
18627	Per2	period homolog 2 (Drosophila)	mKIAA0347|mPer2
18628	Per3	period homolog 3 (Drosophila)	2810049O06Rik|mPer3
223775	Pim3	proviral integration site 3	BC026639|Kid1|MGC27707|MGC37517
66968	Plin5	perilipin 5	2310076L09Rik|AI415325|AW109675|Lsdp5|MLDP|PAT-1
66853	Pnpla2	patatin-like phospholipase domain containing 2	0610039C21Rik|1110001C14Rik|Atgl|TTS-2.2
18984	Por	P450 (cytochrome) oxidoreductase	4933424M13Rik|CPR|CYPOR
19013	Ppara	peroxisome proliferator activated receptor alpha	4933429D07Rik|AW742785|Nr1c1|PPAR-alpha|PPARalpha|Ppar
19883	Rora	RAR-related orphan receptor alpha	9530021D13Rik|Nr1f1|ROR1|ROR2|ROR3|nmf267|sg|staggerer|tmgc26
20526	Slc2a2	solute carrier family 2 (facilitated glucose transporter), member 2	AI266973|Glut-2|Glut2
21685	Tef	thyrotroph embryonic factor	2310028D20Rik
53376	Usp2	ubiquitin specific peptidase 2	B930035K21Rik|Ubp41
19791	RN18S	18S Ribosomal RNA	18S

Table S2

Gene pathways associated with metabolites

Process	10Hrs
Glycolysis / Gluconeogenesis	5.00E-10
Metabolism of xenobiotics by cytochrome P450	2.44E-4
Ascorbate and aldarate metabolism	3.82E-4
Pyrimidine metabolism	5.26E-3

Table S3

UMLS ID	Disease	Log_2 Enrichment
C0017920	Glycogen Storage Disease Type I	2.80
C0015499	Factor V Deficiency	2.80
C0231341	Aging, Premature	2.80
C0042880	Vitamin K Deficiency	2.80
C0020623	Hypolipoproteinemias	2.64
C0029128	Optic Disk Drusen	2.54
C0009940	Convalescence	2.54
C0751895	Vasospasm, Intracranial	2.54
C0020479	Hyperlipoproteinemia Type III	2.54
C0877792	Sleep Disorders, Circadian Rhythm	2.45
C0023817	Hyperlipoproteinemia Type I	2.39
C0272375	Antithrombin III Deficiency	2.32
C0398625	Protein C Deficiency	2.28
C0282513	Aphasia, Primary Progressive	2.28
C0007774	Cerebral Arterial Diseases	2.13
C0035312	Retinal Drusen	2.13
C0242666	Protein S Deficiency	2.13
C2717961	Thrombotic Microangiopathies	2.13
C0018991	Hemiplegia	2.13
C0024408	Machado-Joseph Disease	2.13
C0856761	Budd-Chiari Syndrome	2.13
C0236811	Chronobiology Disorders	2.06
C0021290	Infant, Newborn, Diseases	2.04
C0043012	Wakefulness	1.99
C0042850	Vitamin B Deficiency	1.96
C0752140	Intracranial Embolism	1.96
C0023772	Lipid Metabolism, Inborn Errors	1.90
C0028758	Object Attachment	1.90
C0338451	Frontotemporal Dementia	1.88

Supplemental Figure Legends

Figure S1, related to figure 1: SRC-2 binding sites in the murine liver at ZT4 and ZT18.

A) Histogram of the SRC-2 (ZT4) peak interval enrichment at the TSS. **B)** Histogram of the SRC-2 (ZT18) peak interval enrichment at the TSS. **C)** SRC-2 (ZT4) binding sites determined by CEAS analysis in the mouse hepatic genome. **D)** SRC-2 (ZT18) binding sites determined by CEAS analysis in the mouse hepatic genome **E)** Snapshots of circadian target genes selected for alignment of SRC-2 (ZT4), SRC-2 (ZT18), and SRC-2 (KO) binding sites taken from the USCS genome browser (http://genome.ucsc.edu/cgi-bin/hgGateway) **F)** hd-qPCR of *SRC-2* expression across ZT 2, 6, 10, 14, 18, and 22 in liver, BAT, WAT, heart, muscle, and quantitation of *in situ* hybridization of *SRC-2* in the SCN. **G)** 24-hour SRC-2 hepatic ChIP in *SRC-2*$^{-/-}$ mice at the *Esrra* promoter.

Figure S2, related to figure 2: SRC-2 occupancy enriches with BMAL1 for circadian and metabolic targets.

A) Snapshots of circadian target genes selected for alignment of SRC-2 (ZT4) and BMAL1 (CT4) (Koike et al., 2012) binding sites taken from the USCS genome browser (http://genome.ucsc.edu/cgi-bin/hgGateway). **B)** SRC-2 hepatic ChIP at ZT6 in WT and *SRC-2*$^{-/-}$ mice at the *Per1* promoter or untr10 (negative control). **C)** SRC-2 ChIP at ZT6 in WT and ZT6 *Bmal1*$^{-/-}$ mice and ZT18 in WT and ZT18 *Bmal1*$^{-/-}$ mice on the *SRC-2* promoter. **D)** BMAL1 ChIP at ZT6 in WT and ZT6 *SRC-2*$^{-/-}$ mice and ZT18 in WT and ZT18 *SRC-2*$^{-/-}$ mice on the *SRC-2* promoter. **E)** SRC-2 hepatic ChIP at ZT6 in WT and *SRC-2*$^{-/-}$ mice at the *SRC-2* promoter. **F)** Luciferase assay of the *SRC-2* promoter with expression constructs for SRC-2, BMAL1, and CLOCK in HepG2 cells. **G)** Luciferase assay on the *SRC-2* promoter with acute knockdown with siRNA targeting BMAL1. **H)** Relative mRNA expression by qPCR of *Bmal1* in siControl and siBMAL1 cells. **I)** Luciferase assay on the *SRC-2* promoter with acute knockdown with siRNA targeting SRC-2. **J)** Relative mRNA expression by qPCR *SRC-2* from siControl or siSRC-2 treated cells. **K)** *In vivo* co-immunoprecipitation of BMAL1/SRC-2 and CLOCK/SRC-2 at ZT6 in the liver. **L)** *In vitro* pull-down of BMAL1 with GST or GST-SRC-2 fragments using purified full length BMAL1. Data are graphed as the mean ± s.e.m. **p<0.01 versus WT mice.

Figure S3, related to figure 3: Daily *Tau* values of L/D activity and loss of SRC-2 results in altered central circadian clock gene expression in the SCN.

A) Daily *Tau* values associated with L/D wheel running activity in WT and *SRC-2*$^{-/-}$ male mice (N = 6). **B)** Periodograms for WT mice in Figure 3A. **C)** Periodograms for *SRC-2*$^{-/-}$ mice in Figure 3A**. D)** Temporal expression of genes measured by qPCR in the SCN of entrained in WT and *SRC-2*$^{-/-}$ mice at CT 4, 10, 16, and 22 (N = 3-4). The maximal value from each analyzed gene was normalized to 1. Data are graphed as the mean ± s.e.m. *p<0.05 versus WT mice.

Figure S4, related to figure 4: Loss of SRC-2 results in aberrant peripheral circadian clock and metabolic gene expression in brown and white adipose tissues.

A) qPCR analysis of temporal gene expression in liver from entrained WT and *SRC*-2 liver-specific knockout (LKO) littermate male mice **B)** hd-qPCR analysis of temporal gene expression in BAT from entrained WT and *SRC-2*$^{-/-}$ littermate male mice. **C)** hd-qPCR analysis of circadian gene expression in WAT from entrained WT and *SRC-2*$^{-/-}$ littermate male mice. **D)** hd-qPCR analysis of temporal circadian and metabolic gene expression in the heart from entrained WT and *SRC-2*$^{-/-}$ littermate male mice. **E)** hd-qPCR analysis of circadian and metabolic gene expression in skeletal muscle from entrained WT and *SRC-2*$^{-/-}$ littermate male mice. The maximal value from each analyzed gene was normalized to 1. Data are graphed as the mean ± s.e.m. *p<0.05, **p<0.01, ***p < 0.001 versus WT mice (N = 3-5).

Figure S5, related to figure 5: SRC-2 ablation impacts the hepatic metabolome. A) Heat map of metabolites altered at ZT2 between WT and *SRC-2*$^{-/-}$ mice. **B)** Heat map of metabolites altered at ZT18 between WT and *SRC-2*$^{-/-}$ mice. *p<0.05 versus WT mice.

Figure S6, related to figure 6: SRC-2 deletion significantly disrupts the cell-autonomous clock.

A) qPCR analysis of *SRC-2* knockout as compared to Ad-GFP and Ad-Cre-GFP treated MEFs. **B)** Real time bioluminescence analysis of Ad-GFP and Ad-Cre-GFP treated MEFs infected with Per2-luc construct (Lee et al., 2011b) **C)** qPCR analysis of expression profiles of circadian genes after 4 hours of synchronization in primary hepatocytes isolated from WT and *SRC-2*$^{-/-}$ (N = 3) male littermate mice. Data represent two sets of triplicates of pooled hepatocytes and WT normalized to 1. Data are graphed as the mean ± s.e.m. *p<0.05

versus WT mice. **D)** Heat map of metabolites altered at Hour 2 between Ad-GFP and Ad-Cre-GFP treated MEFs. **E)** Heat map of metabolites altered at Hour 18 between Ad-GFP and Ad-Cre-GFP treated MEFs.

Table S1, related to figure 3: hd-qPCR gene list.

List of genes on the hd-qPCR array used to examine temporal expression of circadian, NR, and metabolic genes in the liver, BAT, WAT, heart, and skeletal muscle across a 24 hour period.

Table S2, related to figure 6: Enriched pathways from the Ad-GFP and Ad-Cre-GFP treated MEFs from the phenotyping array.

Functional analysis on gene sets (R-package GSA) enriched in carbon metabolism using KEGG-derived pathways.

Table S3, related to figure 2: Enriched diseases from the overlapping SRC-2 and BMAL1 binding sites.

Analysis on gene sets enriched using Genopedia on the HuGE Navigator.

Methods Summary

Immunoblot

Immunoblot analyses were performed as described previously (Nishihara et al., 2003). Briefly, proteins separated by SDS-PAGE were transferred to nitrocellulose membranes, blocked in TBST buffer supplemented with 5% bovine serum albumin (BSA) and incubated overnight with primary antibody. Blots were incubated with an appropriate secondary antibody coupled to horseradish peroxidase, reacted with ECL reagents per the manufacturer's (Thermo) suggestion and detected on X-ray film by autoradiography.

Co-immunoprecipitation and *In vitro* Pull-down

For co-immunoprecipitation, HepG2 cells were synchronized with 50% horse serum for two hours (Balsalobre et al., 1998) and for *in vivo* co-immunoprecipitation, protein was isolated from the livers of entrained mice at ZT6 and ZT18, respectively. Lysate was incubated with SRC-2 (BD), BMAL1 (Abcam), CLOCK (Cell Signaling), or IgG (Cell Signaling) antibodies followed by the addition of Protein A Dynabeads (Life Technologies). Eluted

proteins were separated by SDS-PAGE, transferred to nitrocellulose membranes and immunoblotted for SRC-2, BMAL1, and CLOCK.

For the *in vitro* pull-down, equal concentrations of the GST-SRC-2 fragments (Li, 2003), as determined by Coomassie staining, were incubated with full-length recombinant BMAL1 (Ye et al., 2011). After incubation, proteins were washed repeatedly with PBS and 10% input of BMAL1 was used as a loading control. Fragments were separated by SDS-PAGE and then immunoblotted for detection of BMAL1 (Abcam).

Plasmids and Constructs

Cloning of the *SRC-2* luciferase reporter construct was accomplished by PCR amplification of WT mouse genomic DNA using the Phusion High-Fidelity PCR kit (FINNZYMES) with the primer pairs: 5'-ggtacCATGGAGTTCTTTACGCTACTG-3' and 5'- gaagatcTGTTCCCGTGTTAATAACTGCTG-3'. The resulting PCR product was digested with *BglII* and subcloned into pGL3-basic vector (Promega), which was digested with *Acc65i* and blunted with Klenow Enzyme followed by *BglII* digestion. The integrity of the final construct was verified by DNA sequencing. The resulting construct was designated as pGL3-*SRC-2* (-1933 to +61).

Luciferase Assays

For transient-transfection assays, HepG2 cells were plated overnight and transfected with expression plasmids for SRC-2, BMAL1, CLOCK, Cry1 and the pGL3-Basic-*Per1* (-7,200 to +20) or pGL3-*SRC-2* (-1933 to +61) plasmids containing the luciferase reporter using Fugene 6 (Promega) or with siRNA against BMAL1 (Silencer Select), SRC-2 (Thermo Scientific), or Control (Silencer Select) using Lipofectamine (Life Technologies). Cell lysates were prepared 48 hours post-transfection, and luciferase activities were measured with a luciferase assay kit (Promega) and normalized to total protein. Lumicycle analysis was performed using a Lumicycle (Actimetrics). MEFs were cultured with 0.1 mM Luciferin in 35 mm tissue culture dishes.

Running Wheel Analysis

Locomotor activity of WT and *SRC-2*$^{-/-}$ mice (N=6) individually housed with MiniMitter running wheels was recorded using the VitalView® Data Acquisition System. Mice were entrained for at least two weeks in 12 hour L/D cycles under constant temperature and humidity. Mice were then placed under free running conditions (24 hour D/D) cycles for 1 week.

Non-Radioactive *In situ* hybridization (ISH)

WT mice were entrained and whole brain tissue was isolated at ZT 2, 6, 10, 14, 18 and 22. Tissue was serially sectioned at 25 μM (N=3-4). Non-radioactive ISH was performed and quantified as previously described with the *SRC-2* probe (Carson et al., 2005; Yaylaoglu et al., 2005).

Metabolic Profiling

Comprehensive Lab Animal Monitoring System (CLAMS) Calorimetry (Columbus Instruments) was used for 24 hour monitoring of food intake. WT and *SRC-2*$^{-/-}$ mice were acclimated to the chambers for at least one week and *ad libitum* food intake was monitored for 72 hours.

Nanoliter High definition Real-Time qPCR (hd-qPCR)

Liver, skeletal muscle, heart, WAT, and BAT were collected from entrained WT and *SRC-2*$^{-/-}$ littermate male mice and flash frozen at designated ZTs. mRNA was isolated using the RNeasy Mini Kit (Qiagen). Reverse transcription and hd-qPCR were performed on a WaferGen Biosystems SmartChip System (Chen et al., 2012). Data were normalized to 18S. Similar results (data not shown) were obtained in a parallel experiment using the Applied Biosystems/LifeTechnologies Open Array QuantStudio 12K Flex instrument.

qPCR

Total mRNA was isolated from WT primary hepatocytes, murine embryonic fibroblasts (MEFs), liver, or the SCN with RNeasy Kit (Qiagen). Reverse transcription was carried out using Superscript III (Life Technologies) per the manufacturer's instructions. For gene expression analyses, qPCR was performed using the Taqman system with sequence-specific primers and the Universal Probe Library (Roche). All data were analyzed with 18S as the endogenous control. All qPCR primer sequences are available upon request.

Primary Hepatocytes

Primary hepatocytes were isolated from WT and *SRC-2*$^{-/-}$ male littermate mice (N = 3), pooled and plated in triplicate as previously described (Chopra et al., 2008; Matsumoto, 2006). Primary hepatocytes were synchronized with 50% horse serum for two hours (Balsalobre et al., 1998). Cells were isolated for RNA at

Hour 4 in two sets of triplicate using the RNeasy Mini Kit (Qiagen). WT fold induction was normalized to 1 and *SRC-2*$^{-/-}$ hepatocytes fold induction relative to WT was plotted.

Plasma Analysis

Non-esterified fatty acids (NEFAs), triglycerides, and cholesterol were measured at the Mouse Metabolic Phenotyping Core at the University of Cincinnati (http://mousephenotype.uc.edu/UC/).

Mouse Embryonic Fibroblasts (MEFs)

MEFs were isolated from *SRC-2*$^{flox/flox}$ embryos as previously described (Xu, 2005). Cells were transfected with pBSSVD2005 (Addgene plasmid 21826) expressing the SV40 large T antigen. Cells were grown to confluency and split 1/10 for 5 passages to dilute slow growing, senescent cells essentially as described previously (Harding et al., 2009). *SRC-2*$^{-/-}$ MEFs were obtained by infecting *SRC-2*$^{flox/flox}$ MEFs with adenovirus harboring an expression cassette for CRE recombinase. WT MEFs were infected with the corresponding control GFP adenovirus purchased from the Vector Development Core at Baylor College of Medicine. MEFs were plated in triplicate and synchronized. Time zero was set when normal media was added to the cells. Cells were isolated for RNA at 0-40 hours using the RNeasy Mini Kit (Qiagen).

Metabolomic Phenotyping Microarrays

Screening was performed using 96-well plate phenotype microarrays (Biolog, Inc.) containing 88 different carbon substrates and 5 nucleotides as the energy source (Lee et al., 2011a; Putluri et al., 2011a). *SRC-2*$^{flox/flox}$ MEFs infected with either Ad-Cre-GFP or Ad-GFP were seeded at an initial density of $2x10^4$ cells per well in triplicate. Biolog Redox Dye Mix MA was added to each well according to the manufacturer's instructions and kinetic usage of the metabolites were monitored using the GEN III OmniLog ID System (Biolog, Inc.).

Metabolomic profiling

Reagents and internal standards: High-performance liquid chromatography (HPLC) grade acetonitrile, methanol and water were purchased from Burdick & Jackson (Morristown, NJ). Mass spectrometry grade formic acid and internal standards namely, (Zeatine, [15N]-Tryptophan, [D4] Thymine, [15N] Anthranilic acid and N-Acetyl Aspartic acid -d3) were purchased from Sigma-Aldrich (St. Louis, MO). The calibration solution

containing multiple calibrates in acetonitrile/trifluroacetic acid/water was purchased from Agilent Technologies (Santa Clara, CA).

The metabolomics analyses of all samples were executed using the protocol described previously (Putluri et al., 2011a; 2011b; Sreekumar et al., 2009). The raw data (LC-MS output) were normalized using internal standards. Prior to normalization, the median coefficient of variation (CV) of each internal standard was measured to select the appropriate standard for normalization in order to confirm consistency. A number of internal standards, including injection standards, process standards, and alignment standards were used to assure QA/QC targets were met and to control for experimental variability. Aliquots (200 µL) of 10 mM solutions of isotopically labeled standards were mixed and diluted up to 8000 µL (Final concentration 0.25 mM) and aliquoted into a final volume of 20 µL. The aliquots were dried and stored at -80^{o}C until used further. The reproducibility of the profiling process was addressed at two levels; one by measuring only instrument variation, and the other by measuring overall process variation. To monitor instrument performance, 20 µL of a matrix-free mixture of the internal standards described above, reconstituted in 100 µL of methanol:water (50:50) was analyzed by MRM. In addition, the processes of metabolite extraction from the sample were monitored using pooled liver samples and spiked internal standards. In case of the former, 100 mg of pooled liver was extracted in tandem with the cell lines using buffer containing spiked internal standards as described above. In addition, internal standards were also spiked into cell lines during the extraction process. Importantly, the matrix-free internal standards and liver samples were analyzed twice daily. To address overall process variability, metabolomic studies were augmented to include a set of nine experimental sample technical replicates (also called matrix, abbreviated as MTRX), which were spaced evenly among the injections for each day.

Sample preparation for mass spectrometry-based examination of metabolome: Cell pellets were stored at -80°C until analysis. For extraction of the metabolome, 100 mg of liver from each group of mice (five replicates) were homogenized in 1:4 ice cold water:methanol mixture containing an equimolar mixture of 5 standard compounds (Zeatine, [15N]-Tryptophan, [D4] Thymine, [15N] Anthranilic acid and N-Acetyl Aspartic acid -d3). This was followed by sequential addition of ice cold chloroform and water in 3:1 ratio and separation of the organic (methanol and chloroform) and aqueous solvents (water:methanol:chloroform:water; ratio 1:4:3:1). The aqueous extract was de-proteinized using a 3 KDa molecular filter (Amicon Ultracel -3K Membrane, Millipore Corporation, Billerica, MA) and the filtrate containing metabolites was dried under vacuum

Genevac EZ-2plus (Gardiner, NY). Prior to mass spectrometry, the dried extract was resuspended in an identical volume of injection solvent composed with appropriate mobile phase and subjected to liquid chromatography (LC) mass spectrometry.

Liquid Chromatography/Mass Spectrometry (LC/MS): The chromatographic separation of metabolites was performed using either reverse phase (RP) separation or normal phase online with 6490 triple Quadrupole QQQ mass spectrometers Agilent Technologies (Santa Clara, CA).

Separation of Amino acids, CoA's and Carnitines: Targeted profiling (SRM) for the Amino acids, CoA's and Carnitines in electro spray ionization (ESI) positive mode, the RP chromatographic method employed a gradient containing water (solvent A) and acetonitrile (ACN, solvent B, with both solvents containing 0.1% formic acid). Separation of metabolites was performed on a Zorbax Eclipse XDB-C18 column (50 × 4.6 mm i.d.; 1.8 µm, Agilent Technologies) maintained at 37°C. The gradient conditions were 0-6 minutes-2% B; 6.5 minutes-30% B, 7 minutes-90% B, 12 minutes- 95% B, followed by re-equilibration to the initial starting condition.

Separation of TCA metabolites: Targeting the TCA metabolites, the normal phase chromatographic separation was also used for targeted identification of metabolites. This employed solvents containing water (solvent A), with solvent A modified by the addition of 5 mM Ammonium acetate (pH 9.9), and 100% acetonitrile (ACN) solvent B. The binary pump flow rate was 0.2 ml/min with a gradient spanning 80% B to 2% B over a 20 minute period followed by 2% B to 80% B for a 5 min period and followed by 80% B for 13 minute time period. The flow rate was gradually increased during the separation from 0.2 mL/min (0-20 mins), 0.3 mL/min (20.1-25 min), 0.35 mL/min (25-30 min), 0.4 mL/min (30-37.99 min) and finally set at 0.2 mL/min (5 min). Metabolites were separated on a Luna Amino (NH2) column (4 um, 100A 2.1 x 150 mm, Phenominex) that was maintained in a temperature-controlled chamber (37^{o}C). All the columns used in this study were washed and reconditioned after every 50 injections.

Separation of TCA metabolites: Targeted profiling (SRM) for the amino sugars, the RP chromatographic method employed a gradient containing water (solvent A) and acetonitrile (ACN), solvent B, with both solvents containing 0.1% formic acid in case of positive ESI; 1 mM ammonium acetate and 0.05% ammonium hydroxide in case of negative mode ESI. Separation of metabolites was performed on a Synergi-4u- Max-RP 80A (4 µm,

4.6 X 250 mm; Phenominex, CA) maintained at 40°C. The binary pump flow rate was 0.2 ml/min with a gradient spanning 5% B to 10% B over a 15 minute, hold 10% B for 2 minutes 10% B to 90% B over 3 min, 90% B to 5% B over 3 minute, hold 5% B for 5 minutes time period.

Separation of Fatty acids: Targeted profiling (SRM) for the fatty acids, the RP chromatographic method employed a gradient containing water (solvent A) with 10 mM ammonium acetate (pH 8) and 100% methanol (solvent B). Separation of metabolites was performed on a Luna Phyenyl Hexyl (3 um, 2 X 150 mm; Phenominex, CA) maintained at 40°C. The binary pump flow rate was 0.2 ml/min with a gradient spanning 40% B to 50% B over a 8 minute, 50% B to 67% B over 5 min, hold 67% B for 9 min, 67% B to 100% B over 1 min, hold 100%B for 6 minutes time period, 100% B to 40% B over 1 minute and hold 40% B for 7 minutes time period.

Separation of Nucleotides: Targeted profiling (SRM) for the nucleotides, the RP chromatographic method employed a gradient containing water (solvent A) and acetonitrile (solvent B) with both solvents containing 0.1% formic acid. Separation of metabolites was performed on a SB-CN (1.8 μm, 3 X 100mm; Agilent Technologies) maintained at 37°C. The binary pump flow rate was 0.3 ml/min with a gradient spanning 2% B hold for 6 min, 2% B to 30% B over a 0.5 minute, 30% B to 90% B over 0.5 min, 90% B to 95% B over 5 min, 95% B to 2% B over 1 minute hold 67% B for 7 minutes time period.

As controls to monitor the profiling process, an equimolar mixture of 5 standard compounds as described, and a characterized pool of mouse liver tissues were extracted and analyzed in tandem with the experimental samples. These controls were incorporated multiple times into the randomization scheme such that sample preparation and analytical variability could be constantly monitored. Furthermore, two blank runs were performed following the analysis of each sample to prevent any carryover of metabolites.

The mass spectrometry portion of the unbiased profiling platform is based on a 1290 SL Rapid Resolution LC and a 6490 triple Quadrupole (QQQ) mass spectrometer Agilent Technologies (Santa Clara, CA). The samples were independently examined in both positive and negative ionization modes using a dual Electrospray Ionization (ESI) source. The data acquisition during the analysis was controlled using the Mass Hunter workstation data acquisition software.

Analysis of Metabolic Phenotyping Data

Measurements of metabolic phenotyping microarray data were obtained in 15-minute intervals for the time period 0-3.75 hours after plating the cells. The data were first corrected for background signal, obtained from readings of control wells. Specifically, the average value of the three control wells in each replicate, containing only Biolog media, was subtracted from the value of each metabolite on the corresponding plate. The adjusted values were then Z-score transformed. In the analysis, the 2.5 hour measurements were selected, since after extensive examination of the entire time course data, it was concluded that early time points exhibited high variability as the cells were settling down, while at later time points saturation effects were observed.

The metabolic flux through carbon substrate related pathways in *SRC-2*$^{flox/flox}$ MEFs infected with Ad-GFP vs *SRC-2*$^{flox/flox}$ MEFs infected with Ad-Cre-GFP cell lines were compared using heat maps and boxplots. In addition, gene set analysis (R-package GSA) was used to assess the overall enrichment of carbon substrates by mapping the detected metabolites to their corresponding KEGG-derived pathways. The pathways were ranked according to their Benjamini-Hochberg FDR-corrected P-values.

Statistical Analyses: The raw data (LC-MS output) was separately normalized in each method using the internal standard with lowest CV for that specific method. CoA metabolites, nucleotides, amino acid metabolites, TCA compounds and amino-sugars (positive mode) were normalized using L-Zeatine while amino-sugars (negative mode) and lipids were normalized using L-Tryptophan. The normalized data was log-transformed (log2) and used for one-way ANOVA (checking significance of time points in WT and KO groups separately) and two-way ANOVA (considering the type (WT, *SRC-2*$^{-/-}$), time (ZT 2, 10, and 18) and their interaction) based on p-value (FDR adjusted using Benjamini-Hochberg method to adjust for multiple hypotheses). The relative expressions of the metabolites were also presented in the accompanying heat map. All the data analyses were performed using R® statistical software and dependent packages. Results are shown as the mean ± S.E.M. Standard statistical comparison of different groups was performed using two-tailed unpaired Student's *t*-test and the resulting values were adjusted using Benjamini-Hochberg FDR-corrected P-values.

References

Balsalobre, A., Damiola, F., and Schibler, U. (1998). A serum shock induces circadian gene expression in mammalian tissue culture cells. Cell *93*, 929–937.

Carson, J.P., Eichele, G., and Chiu, W. (2005). A method for automated detection of gene expression required for the establishment of a digital transcriptome-wide gene expression atlas. J Microsc *217*, 275–281.

Chen, H.J., Edwards, R., Tucci, S., Bu, P., Milsom, J., Lee, S., Edelmann, W., Gümüs, Z.H., Shen, X., and Lipkin, S. (2012). Chemokine 25–induced signaling suppresses colon cancer invasion and metastasis. J. Clin. Invest. *122*, 3184–3196.

Chopra, A.R., Louet, J.F., Saha, P., An, J., DeMayo, F., Xu, J., York, B., Karpen, S., Finegold, M., Moore, D., et al. (2008). Absence of the SRC-2 Coactivator Results in a Glycogenopathy Resembling Von Gierke's Disease. Science *322*, 1395–1399.

Harding, H.P., Zhang, Y., Scheuner, D., Chen, J.-J., Kaufman, R.J., and Ron, D. (2009). Ppp1r15 gene knockout reveals an essential role for translation initiation factor 2 alpha (eIF2α) dephosphorylation in mammalian development. Proc. Natl. Acad. Sci. U.S.a. *106*, 1832–1837.

Koike, N., Yoo, S.H., Huang, H.C., Kumar, V., Lee, C., Kim, T.K., and Takahashi, J.S. (2012). Transcriptional Architecture and Chromatin Landscape of the Core Circadian Clock in Mammals. Science *338*, 349–354.

Lee, A.J.X., Endesfelder, D., Rowan, A.J., Walther, A., Birkbak, N.J., Futreal, P.A., Downward, J., Szallasi, Z., Tomlinson, I.P.M., Howell, M., et al. (2011a). Chromosomal Instability Confers Intrinsic Multidrug Resistance. Cancer Research *71*, 1858–1870.

Lee, H.-M., Chen, R., Kim, H., Etchegaray, J.-P., Weaver, D.R., and Lee, C. (2011b). The period of the circadian oscillator is primarily determined by the balance between casein kinase 1 and protein phosphatase 1. Proc. Natl. Acad. Sci. U.S.a. *108*, 16451–16456.

Li, H. (2003). Synergistic Effects of Coactivators GRIP1 and -Catenin on Gene Activation: CROSS-TALK BETWEEN ANDROGEN RECEPTOR AND Wnt SIGNALING PATHWAYS. Journal of Biological Chemistry *279*, 4212–4220.

Matsumoto, M. (2006). Dual role of transcription factor FoxO1 in controlling hepatic insulin sensitivity and lipid metabolism. J. Clin. Invest.

Nishihara, E., Yoshida-Komiya, H., Chan, C.-S., Liao, L., Davis, R.L., O'malley, B.W., and Xu, J. (2003). SRC-1 null mice exhibit moderate motor dysfunction and delayed development of cerebellar Purkinje cells. Journal of Neuroscience *23*, 213–222.

Putluri, N., Shojaie, A., Vasu, V.T., Vareed, S.K., Nalluri, S., Putluri, V., Thangjam, G.S., Panzitt, K., Tallman, C.T., Butler, C., et al. (2011a). Metabolomic Profiling Reveals Potential Markers and Bioprocesses Altered in Bladder Cancer Progression. Cancer Research *71*, 7376–7386.

Putluri, N., Shojaie, A., Vasu, V.T., Nalluri, S., Vareed, S.K., Putluri, V., Vivekanandan-Giri, A., Byun, J., Pennathur, S., Sana, T.R., et al. (2011b). Metabolomic Profiling Reveals a Role for Androgen in Activating Amino Acid Metabolism and Methylation in Prostate Cancer Cells. PLoS ONE *6*, e21417.

Sreekumar, A., Poisson, L.M., Rajendiran, T.M., Khan, A.P., Cao, Q., Yu, J., Laxman, B., Mehra, R., Lonigro, R.J., Li, Y., et al. (2009). Metabolomic profiles delineate potential role for sarcosine in prostate cancer progression. Nature *457*, 910–914.

Xu, J. (2005). Preparation, culture, and immortalization of mouse embryonic fibroblasts. Curr Protoc Mol Biol *Chapter 28*, Unit28.1.

Yaylaoglu, M.B., Titmus, A., Visel, A., Alvarez-Bolado, G., Thaller, C., and Eichele, G. (2005). Comprehensive expression atlas of fibroblast growth factors and their receptors generated by a novel robotic in situ hybridization platform. Dev. Dyn. *234*, 371–386.

Ye, R., Selby, C.P., Ozturk, N., Annayev, Y., and Sancar, A. (2011). Biochemical analysis of the canonical model for the mammalian circadian clock. Journal of Biological Chemistry *286*, 25891–25902.